GSMAC-FEM Analysis of Single-Crystal Growth by Cusp MCZ Method

Chung Hyo Jung*, Takahiko Tanahashi
Faculty of Science and Technology, Keio University, 3-14-1, Hiyoshi, Kouhoku-ku, Yokohama, 223-8522, Japan
Yuji Ogawa
Keyence Corporation, 1-3-14, Higashinakazima, Higashiyodokawa-ku, Oosaka, 533-8555, Japan

We present the numerical analysis of the growth of a silicon (Si) single crystal. In the MCZ (Magnetic-field-applied Czochralski) method, two magnetic fields that stand opposite to each other generate a cusp magnetic field. In this work, the three cusp magnetic fields used for the analysis are an external magnetic field, a surface magnetic field and an internal magnetic field. Each case was evaluated mainly as to the degree of stirring, shaft symmetry and the stability of the flow. As a result, the cusp magnetic field that yielded to best conditions was the internal magnetic field.

Key Words : Fluid Dynamics, Numerical Analysis, Cusp Magnetic Field, Silicon Single-Crystal, GSMAC-FEM

Nomenclature

B_0 : External magnetic field [T]
Ec : Eckert number
e_z : Unit vector in the gravitation direction
Gr : Grashof number
Ha : Hartmann number
j : Electric current density vector [A/m^2]
Pr : Pr andtl number
P : Pressure [Pa]
Re : Re ynolds number
T : Temperature [K]
t : Time [sec]
v : Velocity vector [m/s]
φ : Electric potential

1. Introduction

The CZ (Czochralski) (Kakimoto et al., 1997 ; Evstratov et al., 2001 ; Vizman et al., 2001 ;

---
* Corresponding Author,
  E-mail : jung@tana.mech.keio.ac.jp
  TEL : +81-45-566-1512; **FAX** : +81-45-566-1495
  Faculty of Science and Technology, Keio University, 3-14-1, Hiyoshi, Kouhoku-ku, Yokohama, 223-8522, Japan. (Manuscript **Received** August 25, 2001; **Revised** October 16, 2001)

Wetzel et al., 2001 ; Raming et al., 2001 ; Lan and Chian, 2001 ; Dold et al., 2001) method is generally used for growing single-crystal silicon (Si), a semiconductor material, and over 90% of single-crystal silicon growth in recent years has been by this method. However, as the diameter of single crystal increases, convection tends to become turbulent about a rotating shaft, crystal stripes are generated by the nonsteady variations and a nonaxisymmetric distribution of temperature occurs. These phenomena have become serious demerits of the CZ method as they greatly reduce the quality of single crystals. Thus, noting that molten silicon is conductive, the MCZ (magnetic-field-applied CZ) was introduced, which directly controls molten silicon by using magnetic fields in the CZ method. The cusp magnetic field (Lee and Chun, 1997), one type of MCZ, is the opposing placement of magnetic fields created when two facing circular coils are electrically charged in opposite directions. It would be extremely difficult to conduct experimental measurements using this method as the experiment would have to be performed under high temperatures and magnetic fields. On the

other hand, since numerical analysis does not require a change in equipment every time variables are altered, it is economical in terms of cost and time should any modifications in design or manufacturing process become necessary. Therefore, it is considered effective to determine the optimal magnetic fields as a means of overcoming the problems occurring in the CZ method. Thus, we examine the effects of the magnetic field on the dynamic flow of fluid and its temperature distribution by analyzing the experimental model of Watanabe et al. (1998) by GSMAC-FEM (generalized simplified marker and cell finite-element method) using a biquadratic element. We also examine what type of applied magnetic field is best for growing high-quality crystals.

2. Governing Equation

The governing equation is derived from the formulas of the velocity field, electromagnetic field and temperature field. The velocity field formula consists of the continuity equation and the Navier-Stokes equation. The electromagnetic field formula is derived from the conservation laws of current and Ohm's law, and the temperature field formula is written using the energy equation. After the governing equations are simplified, some assumptions are made and spatial discretization is performed by Galerkin's GSMAC-FEM. At that time, Eq. (2) and (5) are separated into the advection phase and nonadvection phase, where a biquadratic element is used for the advection phase. In order to stabilize the flow, a BTD matrix is added in the advection phase. The formulas for each field are as follows.

(Velocity Field)
$$\nabla \cdot v = 0 \qquad (1)$$

$$\frac{\partial v}{\partial t} = -\nabla p - (v \cdot \nabla) v + \frac{1}{Re}\nabla^2 v$$
$$+ \frac{Ha^2}{Re}j \times B_0 + \frac{Gr}{Re^2}Te_z \qquad (2)$$

(Electromagnetic Field)
$$\nabla \cdot j = 0 \qquad (3)$$

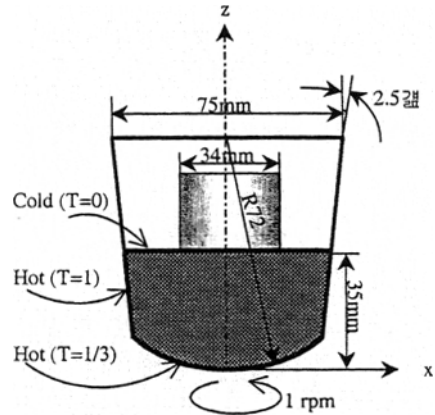Fig. 1 Numerical model

$$j = -\nabla \varphi + (v \times B_0) \qquad (4)$$

(Temperature Field)
$$\frac{\partial T}{\partial t} = -(v \cdot \nabla) T + \frac{1}{PrRe}\nabla^2 T + \frac{Ha^2 Ec}{Re}j^2 \quad (5)$$

The parameters used in the above formulae are defined as v: dimensionless velocity vector, t: dimensionless time, p: dimensionless pressure, Re: Reynolds number, Ha: Hartmann number, j: dimensionless electric current density vector, B_0: dimensionless magnetic flux density vector, Gr: Grashof number, T: dimensionless temperature, e: unit vector, ϕ : electric potential, Pr: Prandtl number, and Ec: Eckert number.

3. Numerical Analysis

3.1 Numerical model
Figure 1 shows the CZ analysis model used for this analysis. This model is based on an experimental model of Watanabe et al. (1998) Although generally a seed crystal is rotated around the pull-up shaft to crystallize acid materials using the CZ method, in this analysis, a crucible is also rotates about the shaft in the direction opposite (Tsuboi et al., 1993) to the rotation of the seed crystal.

3.2 Numerical boundary
Figure 2 shows the numerical grid diagram used for calculation. Since all of the elements are to be shaped into a hexahedron in this analysis, they were specifically arranged so that those with

octagonal boundaries for the horizontal cross section were placed at the center of the circle, and those with circular boundaries at the outside. The total number of elements and nodes are 36,192 and 38,259, respectively.

3.3 Boundary conditions

The following boundary conditions are set for the analysis.

(1) The crucible is rotated at an angular velocity of 1 rpm. The temperature at the bottom of the crucible is made to change linearly from the center of the bottom (dimensionless temperature $T=1/3$) to the lower wall (dimensionless temperature $T=1$) in the radial r direction, and the wall temperature is constant at the dimensionless temperature of $T=1$.

(2) The shape of the free surface is flat. The velocity of the fluid is under the slip boundary condition, and there is no heat transfer via the free surface. The crystal and fluid interface are not rotating and their shapes are constant and flat. The temperature is constant at the dimensionless temperature of $T=0$.

(3) The crucible, crystal and fluid interface, and free surface are nonconductive walls.

3.4 Imposed magnetic field

Figure 3 shows each cusp magnetic field used for the analysis. In this figure, (a), (b) and (c) show the external cusp magnetic field, surface cusp magnetic field, and internal magnetic field, respectively.

3.5 Numerical parameters

Silicon used for analysis was the one at 1687K. In this study, a total of four analyses were performed: no magnetic field (Case 1), external cusp magnetic field (case 2), surface cusp magnetic field (Case 3) and internal cusp magnetic field (Case 4). For comparison, an analysis was also performed for a case where a vertical magnetic field (Case 5) was applied. For the initial conditions, for the analysis with no magnetic field, the velocity, temperature and electric current density were set to zero. The initial conditions for the other cases were determined by the results at the time when the flow was sufficiently developed in Case 1 ($t=120[s]$). The time increment is $\Delta t=5.0\times10^{-3}$, and computation is performed up to the dimensionless time of $t=220$ (approximately $200[s]$). Computational parameters use $Re=4.21\times10^{3}$ and $Pr=1.64\times10^{-2}$ in all cases. The Grashof numbers used are 1.16×10^{7} (Case 1), 2.32×10^{7} (Case 2), and 1.74×10^{7} (Case 3, Case 4, and Case 5). The Hartmann number and Eckert number under the imposed magnetic fields are 1.41×10^{3} and 7.71×10^{-8}, respectively.
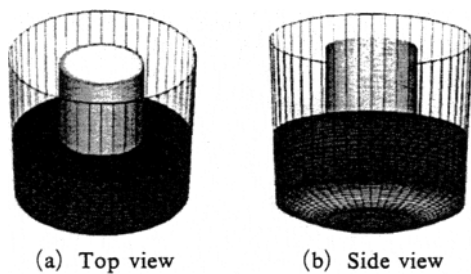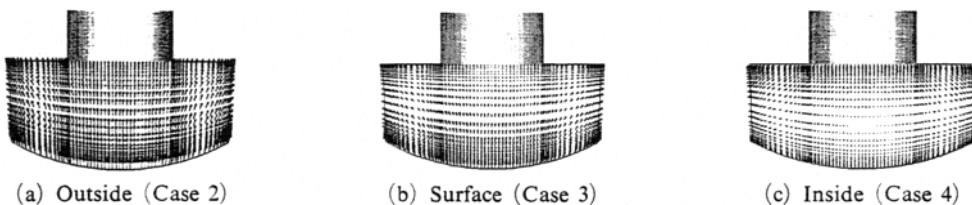
4. Results and Discussion

The following three points are discussed as conditions for forming high-quality crystal.

(1) The entire fluid is thoroughly stirred.

(2) Convection and temperature distribution are axisymmetric.

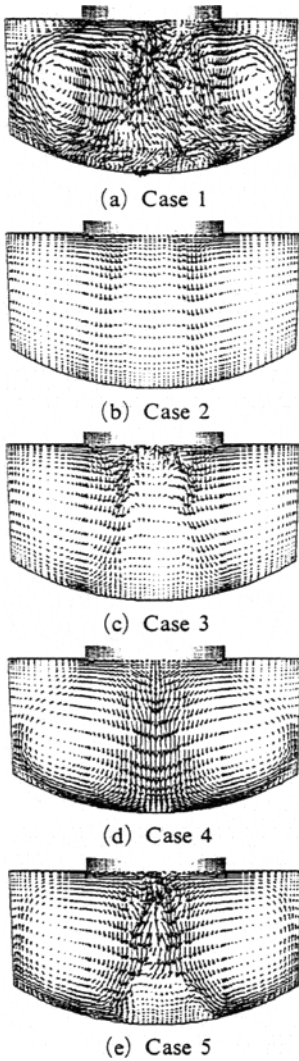(3) Flow is smooth in the vicinity of the crystal interface.

(a) Top view   (b) Side view

Fig. 2 Calculation mesh

(a) Outside (Case 2)   (b) Surface (Case 3)   (c) Inside (Case 4)

Fig. 3 Cusp magnetic fields

Fig. 4   Velocity vectors on x-z plane (t=200)

Fig. 5   Isothermal counters on x-z plane

The results of the velocity field (Fig. 4(a)) and temperature field (Fig. 5(a)) of Case 1 show nonasymmetry, and despite the fact that the flow was in a well-developed state, turbulent flow is apparent around the rotary shaft. The turbulence was caused by the heat convection that was destabilized by the rotation of the crucible. On the other hand, the velocity field indicates the entire fluid was stirred well, and the vortex state is clearly observed. The temperature range of the temperature field (Fig. 5(a)) is a dimensionless temperature of $\Delta T = 0.05$.
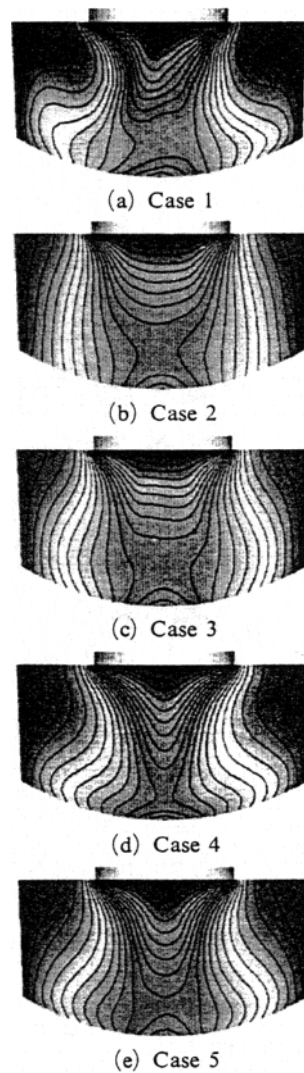
Case 2 is a model where imposed magnetic

fields were placed in such a way that the center of the cusp magnetic field extends to 20 mm above the surface of the fluid. The external current flowing to the coils, which are the source of the magnetic fields, is 1120[A]. The strength of the induced magnetic fields is about 0.15[T] at the bottom of the crucible. From the velocity vectors at the x-z cross section of Fig. 4(b), the state in which the flow is controlled in comparison to Case 1 (without magnetic field) is clearly observed. In the electric current density vector diagram of Fig. 6(a), which shows the x-z cross section from the z direction, the clockwise component

(a) Case 2

(b) Case 3

(c) Case 4

(d) Case 5

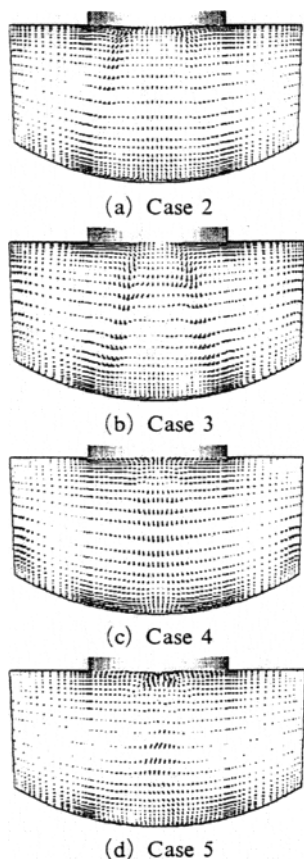**Fig. 6** Current density vectors on x-z plane

$(+\theta$direction component) and the counter-clockwise $(-\theta$direction component) component are nearly equal, thus these components contribute to the inhibition of the convection. Considering the imposed magnetic field placement shown in Fig. 3(a), it can be assumed that the electric currents in the vicinities of the fluid interface and the bottom of the crucible are also contributing to the inhibition of the convection. The flows are concentrated toward the two ends under the crystal. Although the flows are stable and in bilateral symmetry, no stirring of the fluid is observed. These are considered to be inhibiting effects of the magnetic fields on the stirring of the fluid by heat convection and rotation of the crucible.

Case 3 is a model in which imposed magnetic fields are placed so that the center of the cusp magnetic field overlaps the fluid surface. The results in Fig. 6 show that turbulence occurred

under the crystal and it is nonasymmetric. This is because the electric current that flows in the proximity of the fluid interface becomes almost nonexistent as the strength of the magnetic fields at the fluid surface, which is the center of the cusp magnetic field as shown in Fig. 6(b), becomes too weak. In particular, because the components of the x and y directions are extremely weak, there is no inhibition of the convection. Instead, the rotation of the crucible sends the convection and heat to the center to stir the fluid. This is reflected in the cycle structure of the ϕcycle on the isothermal counter at the center part of Fig. 5(c). This cycle structure is consistent with the results (Watanabe et al., 1998) of Watanabe et al.

Case 4 is a model where imposed magnetic fields were placed in such a way that the center surface of the cusp magnetic field extends to 20 mm below the surface of the fluid. Observing the velocity vectors at the x-z cross section of Fig. 4 (d), it can be noted that the flow is orderly compared to that in Case 1. The velocity and temperature fields are stable and axisymmetric, yet the entire fluid is well stirred. These results are considered to be due to the placement of the cusp magnetic fields. By considering the size of the electric current density at the x-z cross section of Fig. 6(c), high electric current densities in the proximity of the fluid interface, the side wall and the bottom of the crucible are observed, and these densities appear to effectively inhibit the convection. What is unique is that the center position of the main whirl created by the convection is considerably deeper than that in other models. The reason why the center position of the main whirl is deeper is considered to be due to the fact that the strength of the magnetic fields becomes zero or extremely weak where the imposed magnetic field is at the center of the fluid.

Case 5 is a model that for comparing the cusp magnetic field application with the vertical magnetic field application. The velocity vectors at the x-z cross section in Fig. 4(c) indicate that the flow inhibiting effects are effective and the flow is stable. Although there is a lack of symmetry of the flow field relative to the central axis, the fluid has

not been stirred. Since no r direction component exists in the vertical magnetic field compared to the cusp magnetic field, the inhibition of the flow component in the direction of magnetic field application at the center of the fluid and the surface of the side wall is not so apparent. This is considered to be the reason why the flow at the center of the fluid is not rectified. It also triggers heat instability in the proximity of the crystal when the hot fluid on the side wall of the crucible flows in the proximity of the crystals.

5. Conclusions

(1) Models in which all the molten silicon in the crucible was stirred were Case 1, Case 4 and Case 5. Models which were axisymmetric were Case 2 and Case 4. Models which were slightly axisymmetric were Case 3 and Case 5, and models in which the flow in the proximity of the crystal was stable were Case 2 and Case 4.

(2) Axisymmetry appeared under magnetic field in the temperature field of silicon, and the following characteristic features were observed in the process. In Case 2, conductivity exceeded convection in the transition of temperature. In Case 3, the cycle structure of the ϕcycle appeared. In Case 4, the in-flow of heat at the side wall surface in the fluid interface was weak. In Case 5, the heat at the side wall surface flowed to the fluid interface.

References

Dold, P., et al, 2001, "Floating Zone Growth of Silicon in Magnetic Fields: IV. Rotating Magnetic Fields," *J. Crystal Growth*, Vol. 231, pp. 95~106.

Evstratov, I. Yu., et al, 2001, "Modeling Analysis of Unsteady Three-Dimensional Turbulent Melt Flow during Czochralski Growth of Si Crystals," *J. Crystal Growth*, Vol. 230, pp. 22

~29.

Kakimoto, K., Eguchi, M. and Ozoe, H., 1997, "Use of an Inhomogeneous Magnetic Field for Silicon Crystal Growth," *J. Crystal Growth*, Vol. 180, pp. 442~449.

Lan, C. W., Chian, J. H., 2001, "Three-Dimensional Simulation of Marangoni Flow and Interfaces in Floating-Zone Silicon Crystal Growth," *J. Crystal Growth*, Vol. 230, pp. 172~180.

Lee, Y. -S., Chun, Ch. -H., 1997, "Experiments on the Oscillatory Convection of Low Prandtl Number Liquid in Czochralski Configuration for Crystal Growth with Cusp Magnetic Field," *J. Crystal Growth*, Vol. 180, pp. 477~ 486.

Raming, G., Mühlbauer, A. and Muhlbauer, A., 2001, "Numerical Investigation of the Influence of EM-Fields on Fluid Motion and Resistivity Distribution during Floating-Zone Growth of Large Silicon Single Crystal," *J. Crystal Growth*, Vol. 230, pp. 108~117.

Tsuboi, H., Tanaka, M., Kobayashi, F. and Misaki, T., 1993, "Three-Dimensional Eddy Current Analysis of Induction Melting in Cold Crucibles," *IEEE Transactions on Magnetics*, Vol. 29-2, pp. 1574 ~1577.

Vizman, D., Friedrich, J. and Müller, G., 2001, "Comparison of the Predictions from 3D Numerical Simulation with Temperature Distributions Measured in Si Czochralski Melts under the Influence of Different Magnetic Fields," *J. Crystal Growth*, Vol. 230, pp. 73~80.

Watanabe, M., Eguchi, M. and Hibiya, T., 1998, "Flow and Temperature Field in Molten Silicon during Czochralski Crystal Growth in a Cusp Magnetic Field," *J. Crystal Growth*, Vol. 193, pp. 402~412.

Wetzel, Th., et al, 2001, "Numerical Model of Turbulent CZ Melt Flow in the Presence of AC and CUSP Magnetic Fields and its Verification in Laboratory Facility," *J. Crystal Growth*, Vol. 230, pp. 81~91.